Monitoring the Interaction between β_2-Microglobulin and the Molecular Chaperone αB-crystallin by NMR and Mass Spectrometry

αB-CRYSTALLIN DISSOCIATES β_2-MICROGLOBULIN OLIGOMERS*

Gennaro Esposito[‡1]**, Megan Garvey**[§2,3]**, Vera Alverdi**[‡2,4]**, Fabio Pettirossi**[‡]**, Alessandra Corazza**[‡]**, Federico Fogolari**[‡]**, Maurizio Polano**[‡]**, P. Patrizia Mangione**[¶‖]**, Sofia Giorgetti**[¶]**, Monica Stoppini**[¶]**, Agata Rekas**[**]**, Vittorio Bellotti**[¶‖]**, Albert J. R. Heck**[‡‡]**, and John A. Carver**[§]

From the ‡*Dipartimento di Scienze Mediche e Biologiche, Università di Udine, 33100 Udine, Italy, the* §*School of Chemistry and Physics, University of Adelaide, Adelaide, South Australia 5005, Australia, the* ¶*Dipartimento di Medicina Molecolare, Istituto di Biochimica, Università di Pavia, 27100 Pavia, Italy, the* ‖*Wolfson Drug Discovery Unit, Centre for Amyloidosis and Acute Phase Proteins, Division of Medicine, University College London, London NW3 2PF, United Kingdom, the* **National Deuteration Facility, Australian Nuclear Science and Technology Organisation, Lucas Heights, New South Wales 2522, Australia, and the* ‡‡*Department of Biomolecular Mass Spectrometry and Proteomics, Bijvoet Center for Biomolecular Research and Utrecht Institute for Pharmaceutical Sciences, University of Utrecht, 3584 Utrecht, The Netherlands*

Background: β_2-Microglobulin (β2m) is a paradigmatic amyloidogenic protein.

Results: *In vitro*, the molecular chaperone αB-crystallin affects the oligomerization and the fibrillogenesis of β2m and its R3A mutant.

Conclusion: αB-crystallin prevents β2m aggregation at various stages of its aggregation pathway.

Significance: Molecular chaperones may be relevant to amyloid formation *in vivo*.

The interaction at neutral pH between wild-type and a variant form (R3A) of the amyloid fibril-forming protein β_2-microglobulin (β2m) and the molecular chaperone αB-crystallin was investigated by thioflavin T fluorescence, NMR spectroscopy, and mass spectrometry. Fibril formation of R3Aβ2m was potently prevented by αB-crystallin. αB-crystallin also prevented the unfolding and nonfibrillar aggregation of R3Aβ2m. From analysis of the NMR spectra collected at various R3Aβ2m to αB-crystallin molar subunit ratios, it is concluded that the structured β-sheet core and the apical loops of R3Aβ2m interact in a nonspecific manner with the αB-crystallin. Complementary information was derived from NMR diffusion coefficient measurements of wild-type β2m at a 100-fold concentration excess with respect to αB-crystallin. Mass spectrometry acquired in the native state showed that the onset of wild-type β2m oligomerization was effectively reduced by αB-crystallin. Furthermore, and most importantly, αB-crystallin reversibly dissociated β2m oligomers formed spontaneously in aged samples. These results, coupled with our previous studies, highlight the potent effectiveness of αB-crystallin in preventing β2m aggregation at the various stages of its aggregation pathway. Our findings are highly relevant to the emerging view that molecular chaperone action is intimately involved in the prevention of *in vivo* amyloid fibril formation.

It is well recognized that there is a close association between a wide range of diseases and protein aggregation. For example, Alzheimer, Parkinson, Creutzfeldt-Jakob, and Huntington diseases are characterized by the accumulation of protein deposits or plaques in which the aggregated protein is arranged in highly ordered amyloid fibrils (1). Understanding the relationship between the formation of amyloid fibrils and protein aggregation diseases is the focus of much research activity. It is clear that amyloid fibril formation arises from the repertoire of partially folded intermediate states of proteins, and there is significant evidence that the process of aggregation of these states causes cellular toxicity which, in turn, contributes to the particular disease (1). Intriguingly, various reports have suggested that the cellular toxicity of the putative causative agent in Alzheimer disease, the amyloid β (Aβ)[5] peptide, and other amyloidogenic proteins, does not arise from the insoluble amyloid deposits but rather from the soluble prefibrillar oligomers (2–6).

Molecular chaperone proteins interact with the intermediate states of proteins. Most likely, they are important in preventing

the accumulation of prefibrillar species *in vivo*, and accordingly, they have been proposed as therapeutics in the treatment of protein conformational diseases (7, 8). In particular, small heat-shock molecular chaperone proteins (sHsps) are attractive in this aspect because of their ability to interact with and stabilize long-lived intermediate states of proteins early on their off-folding pathway, prior to large scale aggregation (8, 9).

$β_2$-Microglobulin ($β2m$) is the nonpolymorphic light chain component of class I major histocompatibility complex (MHC-I) (10). *In vivo*, $β2m$ causes amyloidosis via accumulation in the tissues of patients with renal failure as a result of long term hemodialysis (11). The structure of $β2m$ and the molecular aspects of its amyloid transition have been extensively investigated in recent years, not only because of the clinical relevance of dialysis-related amyloidosis but also as a model for other amyloidogenic proteins (12–19).

Among the amyloidogenic proteins, $β2m$ has the unusual property of not requiring mutation or proteolysis to form fibrils. *In vitro*, however, the transition does not occur spontaneously at neutral pH but requires moderately acidic conditions and proper ionic strength or the presence of chaotropes (20–22). The formation of $β2m$ fibrils at neutral pH occurs upon the addition of seeds and 2,2,2-trifluoroethanol, surfactants, or glycosaminoglycans (23, 24). Furthermore, temperature and pH conditions similar to those occurring upon inflammation in periarticular compartments enhance aggregation (25) and trigger fibril formation in the presence of collagen fibers (26) and heparin (27). The availability of several variants of the natural protein with different stabilities and amyloidogenic properties and the recent finding of a naturally occurring mutation (D76N) leading to a highly amyloidogenic species responsible for a systemic pathology (28) make $β2m$ a convenient system to investigate the unfolding and aggregation processes. For instance, the fragment of $β2m$ devoid of the N-terminal hexapeptide ($ΔN6β2m$) that occurs to a significant extent ($∼30\%$) in *ex vivo* deposits of the protein (13) has an enhanced tendency to aggregate and form fibrils, even at neutral pH (14). Furthermore, the Arg-3-to-Ala mutant of $β2m$ (R3A$β2m$) forms a folded structure very close to that of the wild-type protein, but it exhibits a spontaneous propensity to unfold, aggregate, and precipitate over a period of days to weeks (19).

sHsps are ubiquitous intracellular chaperones. $α$-Crystallin is an sHsp that is composed of two closely related subunits, A and B, each of about 20 kDa in mass. Like most other sHsps, the $α$-crystallin subunits exist as large heterogeneous aggregates of a mass range $∼300–1000$ kDa (29, 30). $α$-Crystallin has been studied for many years because of its presence as the major eye lens protein and its crucial role, via its chaperone ability (31), in preventing crystallin protein aggregation and consequent cataract formation. Interest in $α$-crystallin has increased significantly since the discovery that $αB$-crystallin also occurs extensively outside the lens (32). Its expression levels are enhanced significantly under stress conditions, *e.g.* elevated temperature. The $αB$-crystallin oligomer has an average size of $∼32$ subunits with the dimer as the basic building block (31, 33). The protein is composed of three domains as follows: a central $β$-sheet-containing "$α$-crystallin" domain that is flanked by relatively

disordered N- and C-terminal domains, the latter of which also contains a short, highly mobile, and unstructured C-terminal extension (34–36). Crystal and NMR structures have recently become available for the $α$-crystallin domain (37–39).

In addition to its potent ability to prevent amorphous protein aggregation of numerous target proteins, $αB$-crystallin also inhibits ordered amyloid fibril formation, *e.g.* by the A$β$ peptide (22, 40, 41), apolipoprotein C-II (42), $α$-synuclein, the principal component of Lewy bodies in Parkinson disease (43), $κ$-casein (44–46), ataxin-3 (47), and $β2m$ under acidic conditions (22, 48). Furthermore, $αB$-crystallin inhibits the aggregation of the serpin, $α_1$-antichymotrypsin (49).

This study exploited the complementary insight obtainable from NMR spectroscopy and mass spectrometry (MS) into the early stages of $β2m$ amyloid fibril formation and the nature of the interaction between $αB$-crystallin and $β2m$. For this purpose, we used wild-type $β2m$ and R3A$β2m$ under conditions of a convenient time scale for spectroscopic monitoring of processes that precede and lead to $β2m$ aggregation, along with the effects of $αB$-crystallin on these processes. By use of ^1H NMR spectroscopy, we determined that a nonspecific interaction occurs between the exposed surface of R3A$β2m$ and $αB$-crystallin during chaperone action. Furthermore, MS and NMR diffusion coefficient measurements enabled the $β2m$ oligomerization distribution to be quantified in the absence and presence of $αB$-crystallin. Importantly, $αB$-crystallin induced dis-aggregation of $β2m$ oligomers. It is concluded that $αB$-crystallin is multifaceted in its ability to prevent fibril formation by interacting with $β2m$ at the various stages of its aggregation pathway.

EXPERIMENTAL PROCEDURES

Materials—Recombinant $β2m$ and R3A$β2m$ were prepared as described previously (14, 19). The B subunit of $α$-crystallin was employed for all the experiments except for the DOSY measurements in which bovine eye lens $α$-crystallin (Sigma), composed of $∼3$:1 $αA$-/$αB$-crystallin, was used. Recombinant human $αB$-crystallin was prepared as reported by Rekas *et al.* (43, 50). Protein concentrations were determined spectrophotometrically at 280 nm. For a 1-cm optical path length, $A_{1\%} = $ 16.91 ($β2m$), 17.04 (R3A$β2m$), 6.93 ($αB$-crystallin), and 7.11 ($α$-crystallin). Protein integrity was monitored before and after experimentation by MS.

Thioflavin T Fluorescence Assay—Thioflavin T (ThT) fluorescence assays (440:490 nm excitation/emission) to monitor amyloid fibril formation of R3A$β2m$ (500 $μg/ml$) were undertaken for up to 17 days in 100 mM sodium phosphate buffer at pH 7.4 and 310 K with orbital shaking at 700 rpm in the presence of 10 $μM$ ThT (51).

NMR Spectroscopy—NMR spectra were obtained at 500.13 MHz with a Bruker Avance spectrometer on 0.1–0.9 mM protein samples dissolved in H_2O/D_2O (90:10 and 95:5 v/v) with 50–70 mM phosphate buffer, 50–100 mM NaCl, and pH* in the range 6.5–6.7 (where pH* is the pH meter reading without isotope effect correction). When necessary, samples were centrifuged and/or filtered using filters with a threshold of 0.22 $μm$ (Millipore, Bedford, MA) or 0.02 $μm$ (ANOTOP type, Whatman, Maidstone, UK). Studies were carried out at 310 K apart from a few experiments acquired at 313 K, which did not show

any NMR-detectable differences. The samples containing two proteins were prepared using αB-crystallin/R3Aβ2m at molar subunit ratios of 1:60, 1:15, 1:5, 1:2, and 1:1, and α-crystallin/β2m molar subunit ratios of $1:4.9 \times 10^2$, 1:95, 1:60, and 1:35. The β2m mutant and the stock αB-crystallin solutions employed for measuring the signal attenuations were filtered using 0.02-μm microfilters with either lyophilized or un-lyophilized purified β2m proteins being used. The ^{1}H two-dimensional total correlation spectroscopy (TOCSY) (52) NMR spectra were collected and processed as reported previously (19, 53). Based on the signal-to-noise ratio, amplitude errors typically ranged within $\pm 5\%$, although much larger errors are to be expected for very weak resonances. Values of average accessible surface area of backbone amide and C^α hydrogen atoms were computed with the software available at the public domain biocomputation suite of EMBL, using a probe radius of 0.14 nm and the 20 deposited NMR structure coordinates of R3Aβ2m (19). Molecular structures were generated with InsightII (Accelrys Inc., San Diego), MOLMOL (54), and Swiss-Pdb Viewer software packages.

The diffusion coefficients of a 0.44 mM solution of wild-type β2m at 310 K (93:7 v/v H$_2$O/D$_2$O, 100 mM NaCl, 70 mM phosphate buffer, pH 6.6), as a function of the α-crystallin content (at the ratios reported above), were measured using the convection-compensated two-dimensional <u>d</u>ouble-<u>st</u>imulated <u>e</u>cho <u>d</u>iffusion <u>o</u>rdered <u>s</u>pectroscop<u>y</u> (DSTE DOSY) (55) pulse sequence to record matrices of 2048 (t2) by 80 points (t1). The gradient strength was varied linearly from 2 to 95% of its maximum value (61.1 G/cm). The lengths of the diffusion interval (200 ms) and diffusion gradient (2.5 ms) were optimized to obtain a substantial decay of the signal (95% loss, at least). The data analysis along t1 was performed using the Bruker DOSY software by imposing a single exponential fitting. Water suppression was achieved with the addition of an excitation sculpting WATERGATE module (56, 57).

Mass Spectrometry—MS measurements were performed on lyophilized wild-type β2m solutions dissolved in 100 mM ammonium acetate buffer, pH 6.82, at a final concentration of 120 μM, in the absence or in the presence of αB-crystallin. All sets of measurements were carried out using β2m solutions divided into two equal portions that were or were not filtered through 0.02-μm filters.

For the first set of experiments, β2m was dissolved in a final volume of 500 μl, at the concentrations reported above. The sample was divided into 2 aliquots. The 1st aliquot was the β2m control solution, and the second one was mixed with αB-crystallin in 100 mM ammonium acetate buffer, pH 6.82, at a final ratio of 30:1 β2m/αB-crystallin on a molar subunit basis.

In the second set of experiments, concentrated solutions of αB-crystallin in 100 mM ammonium acetate were added to 50 μl of an aged (20 days old) 120 μM β2m solution at a ratio of 30:1 β2m/αB-crystallin on a molar subunit basis. Before electrospray ionization (ESI), the samples were diluted to a final concentration of 20 μM in 100 mM ammonium acetate buffer, pH 6.82. This concentration was chosen because the physiological concentration of circulating β2m is 0.3 μM in healthy individuals but is elevated 20–60-fold in long term hemodialysis patients (58, 59).

The native MS experiments were performed using an ESI time-of-flight (TOF) LCT mass spectrometer equipped with a Z-spray nanoflow electrospray source (Micromass UK Ltd., Manchester, UK). Aliquots of 2 μl of the 20 μM protein solutions were infused into the mass spectrometer using an in-house pulled and gold-coated borosilicate glass needle.

ESI-TOF-MS parameters were set as follows: capillary voltage, 1.2–1.5 kV; sample cone voltage, 120–150 V; extraction cone voltage, 50 V; source pressure, 6.7 mbar; TOF analyzer, 1.2×10^{-6} mbar. Spectra were recorded in the positive ion mode within the m/z range 500–10,000. For mass calibration, an aqueous 20 mg/ml CsI solution was used. The data were processed with MassLinks Version 4.1 Software (Micromass).

RESULTS

Amyloid Fibril Formation of R3Aβ2m Is Prevented by αB-crystallin—At the global level, amyloid fibril formation of R3Aβ2m was monitored via ThT binding. ThT fluorescence is markedly enhanced upon binding to the cross-β-sheet structure associated with the amyloid fibril structure. The ThT binding curves for an agitated R3Aβ2m solution, in the absence and presence of αB-crystallin, are shown in Fig. 1*A*. Interestingly, the ThT curves reproducibly displayed a biphasic profile, with an initial increase in fluorescence occurring after a lag phase of some 100 h and a plateau phase extending up to about 250 h, followed by a second much larger increase in fluorescence. Transmission electron microscopy images of R3Aβ2m, taken 400 h after the commencement of incubation, confirmed the extensive presence of fibrillar species (data not shown). The presence of increasing amounts of αB-crystallin led to the partial, and at higher concentrations, complete suppression of ThT fluorescence, due to the inhibition of fibril formation. When only partial suppression of ThT fluorescence increase was observed, *i.e.* at αB-crystallin/R3Aβ2m molar subunit ratios of 1:1000, 1:100, and 1:10, little if any inhibition of the first ThT fluorescence increment occurred, whereas the effect on the second ThT fluorescence increment was significant, implying that αB-crystallin preferentially interacts with the second phase of R3Aβ2m aggregation. Fig. 1*B* summarizes the amount of ThT fluorescence at the end of the experiments (400 h).

Assessment of the Stability of R3Aβ2m Solutions in the Presence and Absence of αB-crystallin as Monitored by ^{1}H NMR Spectroscopy—The ^{1}H NMR spectrum of R3Aβ2m has been assigned (19) thereby enabling investigation of alterations in chemical shifts and intensities of its resonances upon interaction with αB-crystallin. Because of its relatively rapid rate of aggregation and precipitation, the mutant exhibits a more convenient aggregation time scale for monitoring by NMR than the wild-type protein.

Depending on the procedures undertaken after expression, purification, and sample preparation, the time scale for R3Aβ2m aggregation was variable. We found that the timing of the onset of precipitation and its extent depended on several factors. Besides the expected effects of protein concentration, pH, ionic strength, and temperature, the onset of precipitation was also affected by filtering the freshly prepared solutions and, specifically, by the exclusion size threshold of the filter (0.22 or 0.02 μm). Different precipitation patterns were also observed
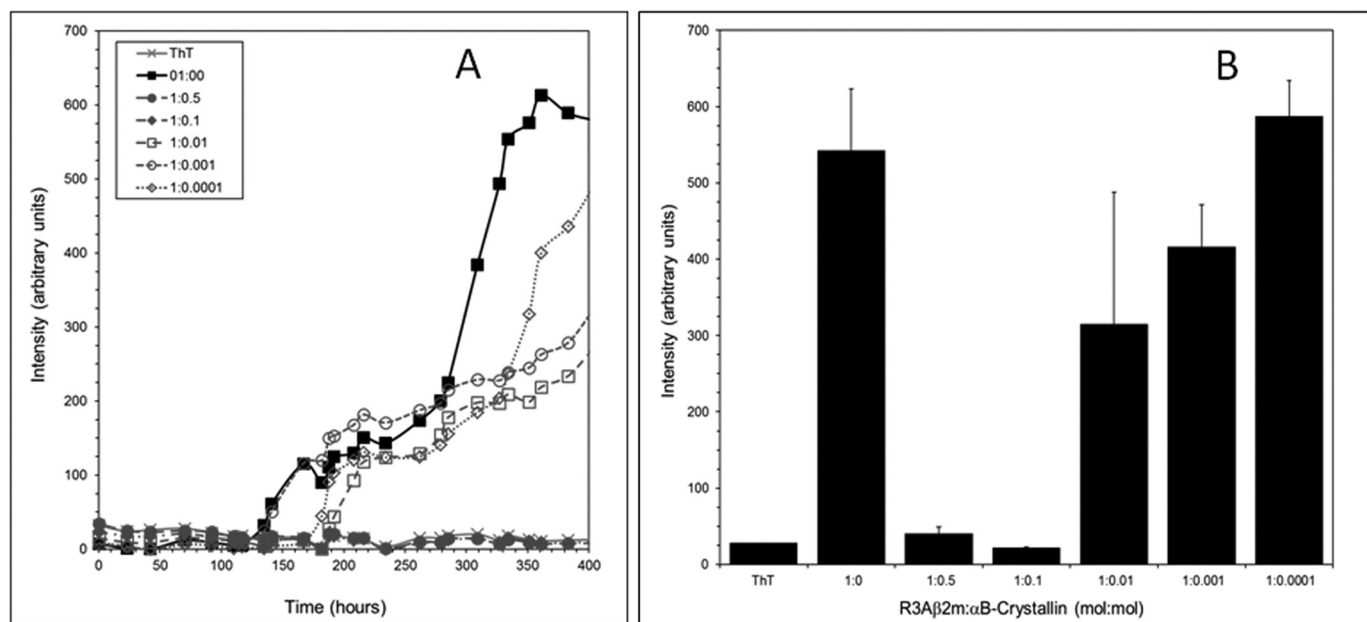
FIGURE 1. *A,* ThT fluorescence of R3Aβ2m in 100 mM phosphate buffer, pH 7.4, and 37 °C with time in the absence and presence of increasing concentrations of αB-crystallin (R3Aβ2m, αB-crystallin values on a molar subunit basis). *B,* ThT fluorescence values of R3Aβ2m after 400 h of incubation in 100 mM phosphate buffer, pH 7.4, and 37 °C in the absence and presence of αB-crystallin, at the indicated molar subunit ratios. All data were derived from four replicates. The *bars* given in *B* are thus the standard mean ± S.E. for *n* = 4.

when the freshly prepared solutions were centrifuged rather than filtered. Other sources of variability were whether the protein had been subjected to lyophilization after final purification by dialysis, as well as omitting the lyophilization step so as to utilize only frozen aliquots of purified protein solutions. Solutions of lyophilized protein that were used unfiltered or subjected to filtration through a 0.22-μm filter prior to use are referred to as *ordinary* samples. Solutions of protein not subjected to lyophilization that had been filtered through the 0.02-μm filter are referred to as *nonordinary* samples.

As already reported (19), the ¹H NMR spectrum of an ordinary solution of R3Aβ2m, acquired immediately after dissolution, shows the same pattern as observed with wild-type protein (12), which is consistent with the strong conformational similarities between the two species (19). Data were collected using clear solutions prepared without filtering and, sometimes, with mild centrifugation. After a lag phase that could last one or several days depending on the concentration and previous history of the sample, the NMR spectrum underwent changes caused by the concomitant processes of unfolding and aggregation followed by precipitation, as reported previously (19). The progress of unfolding is highlighted by gradual loss of the isolated hallmark resonances of the folded species, coupled to a simultaneous growth of resonances at random coil chemical shift values (19) (Fig. 2). Precipitation was readily ascertained by visual inspection of the sample and by a decrease in the total NMR spectral integral.

Fig. 2*A* shows the one-dimensional ¹H NMR spectrum of a 1:1 mixture (on a molar subunit basis) of an ordinary sample of R3Aβ2m and αB-crystallin. αB-crystallin forms a large oligomer of average mass of ~650 kDa (31). The αB-crystallin oligomers tumble very slowly, and therefore the majority of their resonances is not observed in the NMR spectrum. The exception is the flexible and unstructured C-terminal extension of 12

amino acids (34–36) that gives rise to additional, readily detectable cross-peaks at random coil chemical shift values in the fingerprint region of two-dimensional NMR spectra (*e.g.* TOCSY) (Fig. 2*A, insets*). The same pattern was also observed in NMR spectra at half of this ratio, *i.e.* 0.5:1.0 αB-crystallin/R3Aβ2m (data not shown). The spectra shown in Fig. 2*A* are interpreted as evidence for a weak interaction between R3Aβ2m and αB-crystallin that introduces a limited broadening of the R3Aβ2m resonances due to transient mutual association.

Quantification of the effects of αB-crystallin on R3Aβ2m spectra was undertaken by integration of selected resonances and cross-peaks in the one- and two-dimensional TOCSY spectra. Fig. 2*B* documents the time-dependent intensity change of an upfield-shifted methyl peak of R3Aβ2m (L23 δ_1-CH$_3$). Similar results are shown also for amide cross-peaks from the two-dimensional TOCSY fingerprint (Fig. 2, *C* and *D*). In the absence of αB-crystallin, after a lag phase of ~50–60 h, the resonance intensity decreased in a linear time-dependent manner and achieved about 80% loss over the time course of the experiment (~195 h). In the presence of αB-crystallin, for the same resonance, the loss of intensity was slowed down 3.4-fold, on average (Fig. 2*B*). No detectable lag phase also occurred in the presence of αB-crystallin. Overall, in the presence of αB-crystallin, a 6-fold reduction in the increase in intensity of the aliphatic resonances that are characteristic of unstructured peptides was measured, compared with the corresponding measurements in the absence of aB-crystallin under the same conditions (data not shown). Moreover, the samples with αB-crystallin present exhibited hardly detectable precipitation over the same time period compared with samples without αB-crystallin, where significant precipitation occurred.

In the absence of αB-crystallin, the timing for the lag phase and subsequent loss of NMR resonance intensity (Fig. 2, *B* and
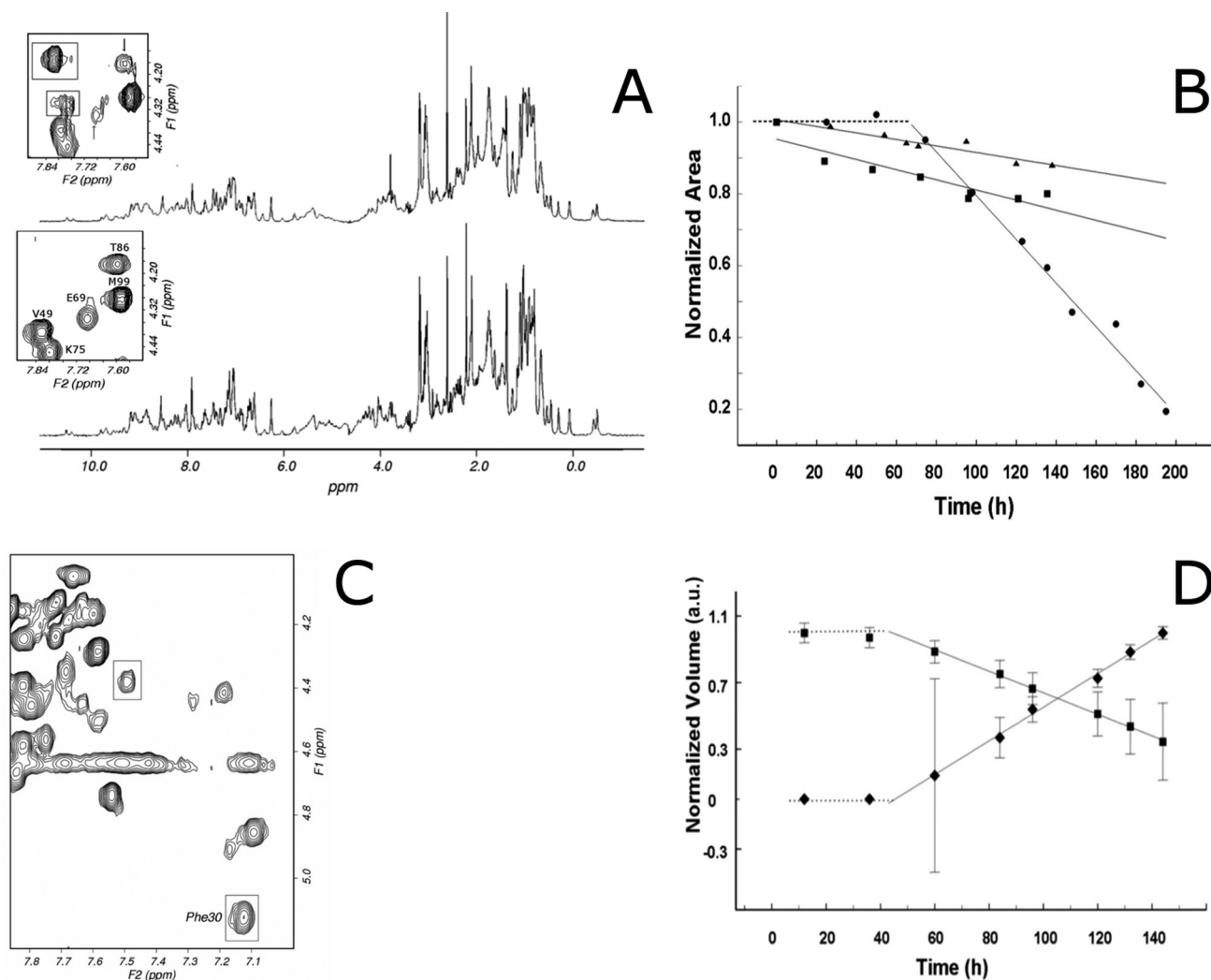
FIGURE 2. *A,* 500 MHz ^{1}H NMR spectra of an ordinary sample of R3Aβ2m (~0.9 mM, 310 K, pH 6.6) in the absence (*lower trace*) and presence (*upper trace*) of an equimolar amount of αB-crystallin subunit. The only apparent consequence of the sHsp addition is a general broadening, with conservation of the spectral pattern of R3Aβ2m. The *insets* show a portion of the H^N-H^α connectivity (fingerprint) region of the corresponding two-dimensional TOCSY spectra. The *boxed* cross-peaks arise from the unstructured and flexible C-terminal extension of αB-crystallin. Only this region of 12 amino acids is present in the spectrum by virtue of its fast local tumbling as opposed to the extremely slow overall motion of αB-crystallin oligomer (~650 kDa) that causes the extreme broadening of other resonances (34–36, 60). Assignments are indicated for R3Aβ2m NH to α-CH cross-peaks (12, 19). *Arrows* mark visibly attenuated R3Aβ2m connectivities for Q69 and T86. *B,* time evolution of the resolved upfield-shifted methyl resonance (L23 $δ_1$CH$_3$), which is diagnostic for the correctly folded species, of an ordinary sample of R3Aβ2m obtained from 500 MHz ^{1}H one-dimensional NMR spectra, in the absence (*circles*) and in the presence of αB-crystallin at equimolar (*squares*) or halved concentration (*triangles*) with respect to R3Aβ2m. The average rate of loss of signal intensity was $(5.6 ± 0.5) × 10^{-3}$ h^{-1} in the absence of αB-crystallin and $(1.5 ± 0.5) × 10^{-3}$ or $(1.8 ± 0.5) × 10^{-3}$ h^{-1} for 1:2 or 1:1 αB-crystallin/R3Aβ2m mixtures, respectively. The errors on the rates were estimated by considering the deviations obtained when assessments were made using absolute resonance amplitudes rather than self-normalized values (53) to account for the uncertainties introduced by the scaling procedure. Generally speaking, such uncertainties arise when resonances with smaller linewidths overlap pre-existing signals, as well as from the general linewidth increase upon addition of αB-crystallin. *C,* two-dimensional TOCSY fingerprint details obtained from an 82-h-old solution of R3Aβ2m (0.8 mM, 310 K, pH 6.6). The *boxed* cross-peaks represent the NH-αCH connectivities whose time evolution is displayed in *D,* respectively, from Phe-30, in the folded protein, and from an unknown residue, in the unfolded soluble species. *D,* time dependence of the two-dimensional TOCSY cross-peak amplitudes of *C* (Phe-30 = *squares*, unassigned = *diamonds*). In the absence of αB-crystallin, the evolution of the resolved fingerprint cross-peaks showed typically a similar trend as that obtained by considering the evolution of the resolved methyl resonances in one-dimensional ^{1}H spectra (*B*). Indeed, the slope of the decreasing Phe-30 cross-peak amplitude is $-5.9 × 10^{-3}$ h^{-1}, *i.e.* in absolute value the same, within the experimental error, as the slope of the unknown cross-peak intensity.

D) matches the lag phase and first rise of ThT fluorescence (Fig. 1). Following a latency period of 60 ± 20 h, the NMR signal loss is due to concomitant precipitation and formation of large soluble aggregates that are poorly observable or totally unobservable by NMR due to their very large linewidth. The total loss of the NMR signal occurs around 200–250 h, *i.e.* at the time as the first plateau in the ThT fluorescence data (Fig. 1). So, the initial increase of ThT fluorescence could coincide with the loss of the NMR intensity due to formation of large prefibrillar aggregates.

We hypothesize that these prefibrillar aggregates, possibly containing some extent of intermolecular cross-β-structure, occur along nonamyloid and/or slow amyloid-forming pathways that are present at high β2m concentration and are enhanced by solution agitation (60).

Mapping R3Aβ2m-αB-crystallin Interaction by NMR Spectroscopy—By contrast to the situation in the previous section with ordinary samples of R3Aβ2m, neither unfolding nor precipitation of R3Aβ2m was detected over an extended time
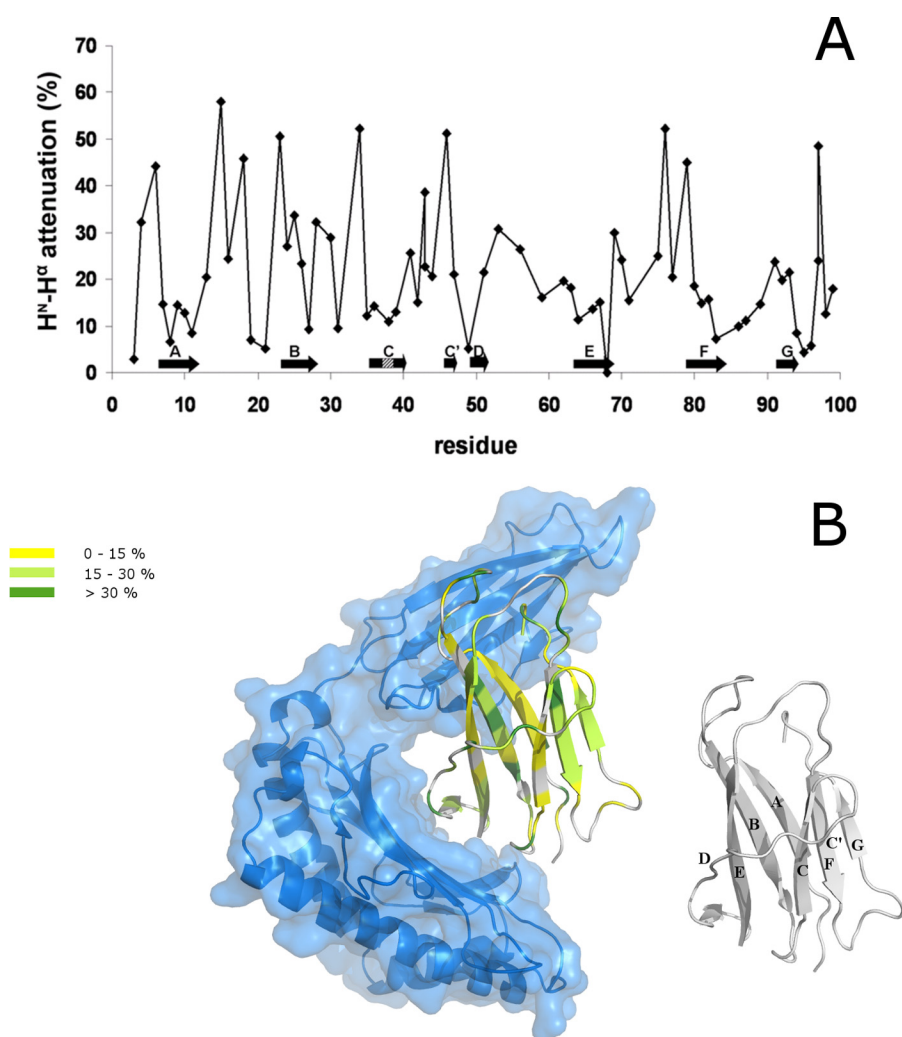
FIGURE 3. *A,* auto-scaled attenuation percentages (53) of R3Aβ2m fingerprint H^N-H^α TOCSY cross-peaks due to the presence of αB-crystallin. Data were obtained from integration of two-dimensional TOCSY spectra of 0.1 mM R3Aβ2m nonordinary samples, in the absence and presence of αB-crystallin at a molar ratio of 1:5 αB-crystallin/R3Aβ2m. Because of resolution limits, only 67 out of 94 expected H^N-H^α connectivities could be integrated. The missing attenuation data were from Ile-1, Gln-2, Arg-12, Asn-17, Ser-20, Phe-22, Gly-29, Ser-33, Val-37, Leu-40, Arg-45, Lys-48, Glu-50, Ser-52, Leu-54, Ser-55, Ser-57, Lys-58, Trp-60, Ser-61, Leu-65, Thr-73, Glu-74, Tyr-78, His-84, Val-85, and Ser-88 cross-peaks, with no amide connectivity occurring for the prolyl residues at positions 5, 14, 32, 72, and 90 and the N-terminal methionine (M0). The attenuations exhibited a qualitatively identical pattern at a 1:15 molar ratio. However, greater attenuation (whose maximum was around 50%), which was more convenient for quantification, was observed at the higher αB-crystallin ratio. The location of the β-strand segments according to the NMR solution structure (19) is given at the *bottom* of the figure. The attenuation trend along the R3Aβ2m sequence exhibited a clear analogy with the results of the experiments performed at an equimolar concentration on an ordinary sample (Fig. 2*A*). *B,* schematic representation of β2m secondary structure showing *A* data, *i.e.* the attenuation levels of R3Aβ2m H^N-H^α TOCSY connectivities due to αB-crystallin interaction observed in nonordinary samples. Class I MHC heavy chain (backbone schematic and space filling) is shown in transparency. The crystal structure coordinates of the complex were used (Protein Data Bank code 3HLA (10)). A three-color code was employed to report R3Aβ2m experimental attenuation, as indicated explicitly. The residue positions for which no attenuation data could be measured is colored *gray*. The small schematic aside shows the β-strand naming scheme of β2m. The drawing was prepared with PyMOL (DeLano Scientific LLC).

period in nonordinary solutions prepared from un-lyophilized protein that had been filtered through 0.02-μm filters. Thus, analysis of NMR spectra of these samples in the presence of αB-crystallin was not affected (over typical measurement time intervals) by systematic uncertainties due to the loss of soluble protein or the onset of resonances with unknown linewidth due to R3Aβ2m aggregation. Therefore, measurements of the attenuation of resonances induced by αB-crystallin were undertaken using αB-crystallin/R3Aβ2m at molar ratios suitable for NMR quantification. Attenuation of two-dimensional TOCSY fingerprint (H^N-H^α) cross-peaks was measured at 1:15 and 1:5 molar subunit ratios (data not shown). Qualitatively, identical patterns were observed at both ratios, and therefore,

only the more precise results at the higher ratio (1:5) are reported (Fig. 3*A*).

To avoid a complex range of local mobilities, the quantitative attenuation analysis was restricted to connectivities from backbone hydrogens, *i.e.* a class of nuclei with relatively homogeneous motional properties (61). The fingerprint resolution of the TOCSY spectrum was not always sufficient to estimate individual cross-peak amplitudes, so only 67 out of 94 H^N-H^α correlations could be integrated, which introduced discontinuity in the data of Fig. 3*A*. The interaction of R3Aβ2m with αB-crystallin is very dynamic due to a weak, nonspecific association between the two proteins. No chemical shift changes occurred, so the observed broadening of cross-peaks is ascribed

to the high effective mass that transiently is experienced by R3Aβ2m upon interaction with the chaperone.

At first glance, the profile of the fingerprint cross-peak attenuations appears to be spread over the whole R3Aβ2m sequence, except for the segment of residues 50–70 where the data set is sparse (Fig. 3B). The attenuations did not show any specific dependence on amino acid type, or any correlation with the secondary and tertiary structure, or a high surface exposure of the NH-C^{α}H moieties. In detail, the largest attenuation values of H^N-H^α correlations were mainly located in the inter-strand loop regions, namely the A-B and E-F loops and the C′ strand (five out of the nine most attenuated H^N-H^α connectivities with an attenuation range of 40–50%). Therefore, the upper apical region of R3Aβ2m (Fig. 3B) may be preferentially involved in the interaction with αB-crystallin. Other backbone nuclei that experience comparable signal amplitude reductions are spread over the molecule. Fig. 3B provides a color-coded structural overview of the involvement of R3Aβ2m regions in interaction with αB-crystallin, as inferred from the NMR data, and shows that the contact patches are disseminated over the whole surface of R3Aβ2m. Among them, the regions of β2m in contact with the heavy chain of MHC-I (in transparent format) are readily apparent (10). Therefore, the weak, nonspecific interaction between R3Aβ2m and αB-crystallin also involves β2m regions with a propensity toward protection from the aqueous environment to limit their hydrophobic exposure.

Assessing the Effect of α-Crystallin on Wild-type β2m Aggregation by NMR Diffusion Measurements—We utilized NMR DOSY experiments (55) to measure the translational diffusion coefficient (D_T) of wild-type β2m as a function of α-crystallin concentration (Fig. 4). At 310 K, a 0.44 mM solution of wild-type β2m reproducibly exhibited a D_T value of 1.83×10^{-10} m²/s that did not change appreciably over 5 days. Assuming a spherical model and using a mass-dependent protein density estimate (62), this value is consistent with an apparent mass of 19.9 kDa. The molecular mass of β2m is 11.9 kDa, implying that the protein undergoes aggregation processes of variable stoichiometry, *i.e.* as per the association equilibria previously proposed (19) with a dimer being the most populated species. In this respect, the conclusion generated by NMR is different from that obtained by MS (see below), which we ascribe to the 4-fold β2m concentration difference between the two experiments. Consistent with this, NMR diffusion measurements with freshly prepared β2m solutions at a much lower concentration (~0.1 mM) generated a D_T value consistent with a mass of 12 kDa in agreement with the MS data on similar samples that showed a predominance of monomeric species.

The diffusion coefficient of a 0.44 mM solution of β2m was also determined by NMR following sequential additions of α-crystallin. The D_T value did not alter for an α-crystallin/β2m ratio of $1:4.9 \times 10^2$, but at ratios of 1:95, 1:60, and 1:35, a D_T value of 1.89×10^{-10} m²/s was obtained (Fig. 4), with a slight increase observed over 7 months after the last addition of α-crystallin to the solution. For the D_T value measured after this last addition, the corresponding apparent mass of β2m was determined to be 17.9 kDa, a value that suggests a small but significant shift of the oligomerization equilibria toward lower mass species in the presence of α-crystallin, a shift that
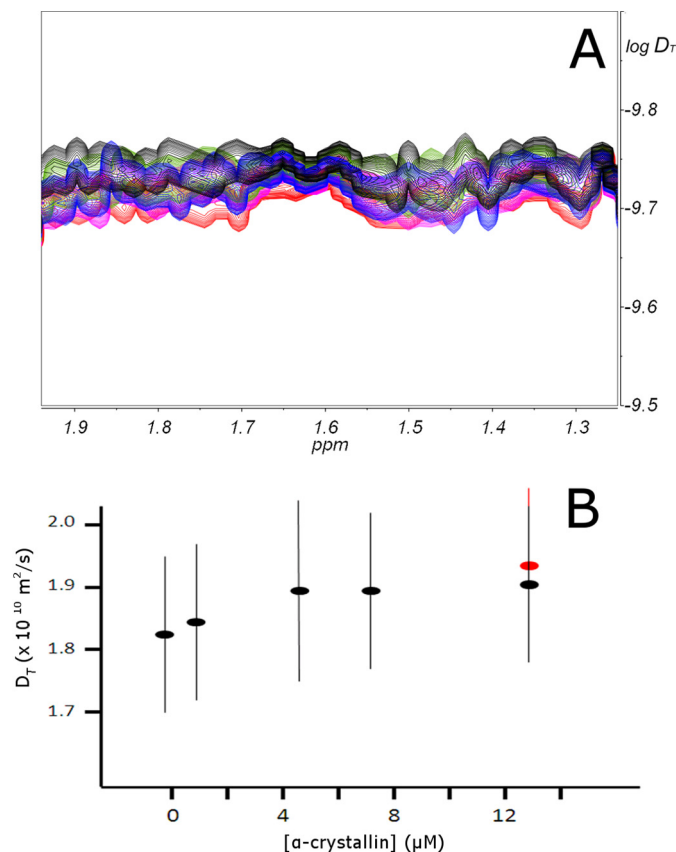

FIGURE 4. *A*, wild-type β2m NMR DOSY spectra as a function of α-crystallin concentration and time. A limited window of the aliphatic region is shown to highlight the small but significant alteration in diffusion coefficient. The contour traces of five different DOSY experiments are superimposed at α-crystallin/β2m molar ratios of 0:1 (*black*), 1:4.9 × 10² (*green*), 1:95 (*blue*), 1:35 (*pink*), and 1:35 after 230 days from the last α-crystallin addition (*red*). The substantial overlap of the traces at the two lowest and highest α-crystallin concentrations reflects the increase in translational diffusion coefficient value, D_T, of β2m below some 100-fold molar excess with respect to α-crystallin. The effect persists with solution aging. *B*, corresponding D_T values of β2m as a function of α-crystallin concentration. The plotted data are the center of gravity measured at 1.6 ppm in the DOSY traces in *A*, with errors representing the maximum excursions above and below the determined value in the same traces. The *red point* refers to the measurement repeated 230 days after the first determination on the freshly prepared solution of 1:35 α-crystallin/β2m.

occurred to a greater extent over the long term (Fig. 4). A control TOCSY spectrum confirmed the stability of the β2m sample whereby α-crystallin preserved the native conformation of β2m as was also observed by NMR spectroscopy for R3Aβ2m in the presence of αB-crystallin (Fig. 3A).

Time Course Oligomerization of Wild-type β2m as Monitored by Mass Spectrometry—The alteration over 20 days in the mass spectrum of wild-type β2m after dissolving the protein in solution at pH 6.8 is reported in Fig. 5. The spectra show time-dependent changes in peak identities and intensities, in particular as new (oligomeric) species are formed in solution. Immediately after dissolution, mainly monomeric and some dimeric β2m species were detected, and after 4 h, oligomers up to hexamers were readily recognizable (data not shown). Later, species with higher mass appeared with increasing intensities, but their unambiguous identification could only be determined up to the octameric species. In Fig. 5, the development with time of increasing peak intensities, corresponding to an increase in
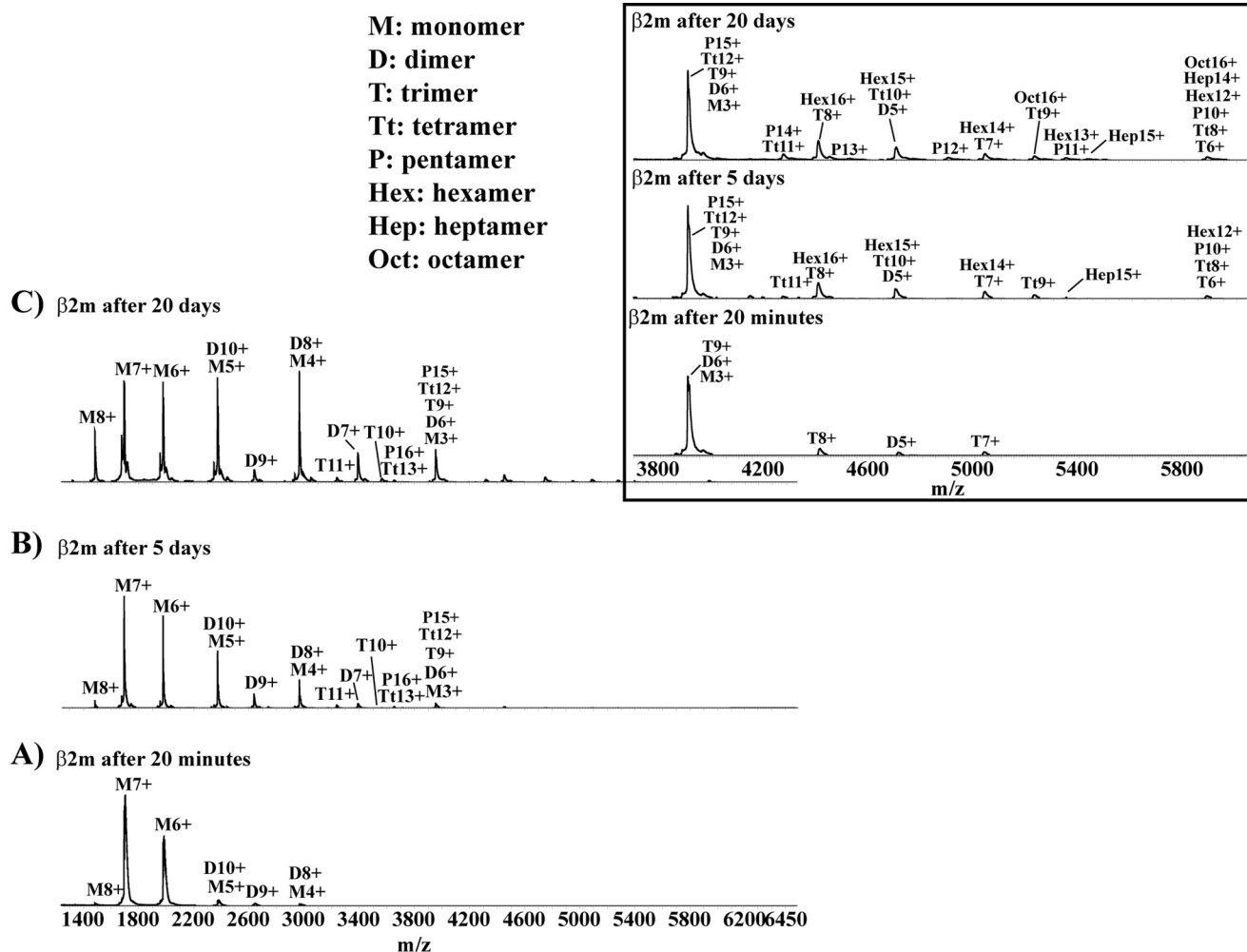
M: monomer
D: dimer
T: trimer
Tt: tetramer
P: pentamer
Hex: hexamer
Hep: heptamer
Oct: octamer

FIGURE 5. **Monitoring the oligomerization of wild-type β2m by ESI-MS over 20 days.** Mass spectra were acquired 20 min (*A*), 5 days (*B*), and 20 days (*C*) after solution preparation. The assignments of the different oligomeric species are given in the figure. The *inset* shows an expansion of the 3800–5800 mass/charge range where the growth in intensity of all the detected oligomeric species can be followed.

concentration of dimer, trimer, tetramer, and the onset of larger aggregated species, is consistent with the formation of oligomers in solution that may be the forerunners of nucleation and fibrillogenesis (19).

To characterize quantitatively the time course of β2m oligomerization, peak areas in the mass spectra were evaluated. Because of the absence of an internal time-independent reference, raw data of areas corresponding to dimers or the sum of higher oligomers, *i.e.* from trimers to octamers, were normalized in each spectrum to the area corresponding to the overall sum of the β2m peaks. This normalization procedure can be considered an internal scaling of the experimental data sets, and thus the intensity data obtained thereof are referred to as autoscaled areas. It should be noted that, despite mass conservation, comparisons among autoscaled areas may be affected by systematic errors due to the failure to detect very large oligomeric species (*i.e.* larger than octamers) in the mass spectra, especially for samples that were aged for a long period.

The time course of signal intensity for mass spectra of the β2m dimer species and the higher oligomer pool, from trimers up to octamers, normalized over the total area sum, was quantified (Fig. 6). The percentage of dimer species present in solu-

tion increased steadily with time reaching 32% of the total 8 days after preparation. A similar trend was seen also for the sum of the other oligomers larger than dimers. In all cases, oligomer autoscaled areas were more intense in the unfiltered than the filtered samples with a 0.02-μm threshold (20-nm-filtered samples). The difference between 20-nm-filtered and unfiltered samples was greater for the oligomer pool compared with the dimeric species (Fig. 6).

Effect of αB-crystallin on Wild-type β2m Oligomerization as Monitored by Mass Spectrometry—To examine the effect of αB-crystallin on β2m aggregation, mixtures of wild-type β2m and αB-crystallin at molar subunit ratios of 30:1, 60:1, and 90:1 β2m/αB-crystallin were prepared and examined by MS. Two sets of experiments were performed. The first set involved the preparation of a fresh mixture of β2m and αB-crystallin in solution, followed by its monitoring over time by MS in tandem with a control solution that contained β2m only. In the second set of experiments, αB-crystallin was added to an aged (20-day-old) solution of β2m, at the same molar ratios listed above.

Fig. 7 shows the mass spectrum with time of the solution containing simultaneously dissolved β2m and αB-crystallin (at a subunit molar ratio of 60:1) as monitored over 20 days (*A–E*)
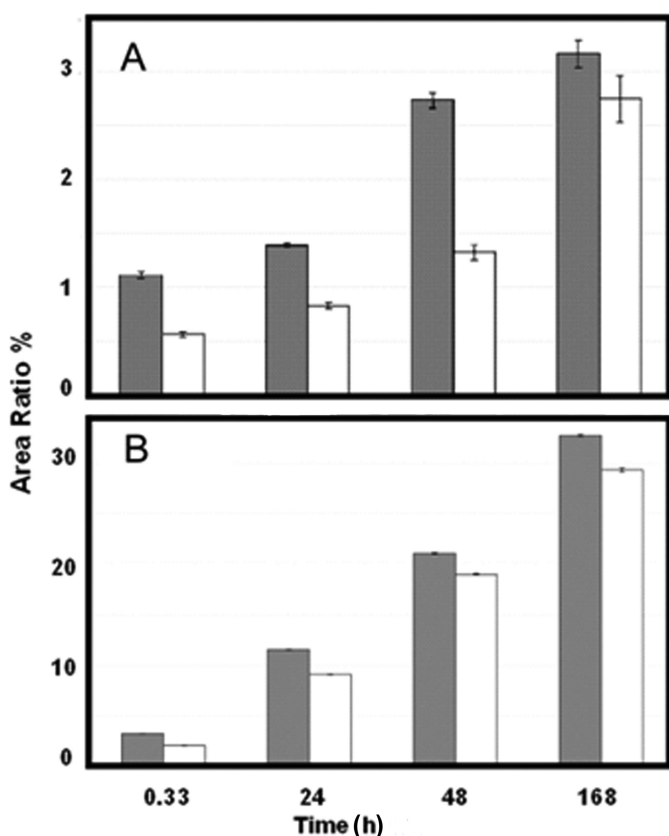
FIGURE 6. **Time course of the autoscaled peak areas, *i.e.* expressed as percentage ratio with respect to the sum of all β2m signals, corresponding to the MS-detected β2m oligomers larger than dimers (*A*) and dimers (*B*).** In particular, the *bars* report the sum of the autoscaled areas of all detected charge state signals for the higher oligomers, *i.e.* trimers, tetramers, etc., up to octamers (*A*), and the autoscaled areas for the dimers (*B*). The results for the ordinary (unfiltered) samples are indicated with *solid bars,* and those from the nonordinary samples (the samples filtered with a 0.02-μm threshold) are indicated with *empty bars.* The percentage of dimer species present in solution increases steadily with time reaching 32% of the total 8 days after preparation (*B*). A similar trend is seen also for the sum of the other oligomers larger than dimers (*A*). In all cases, oligomer autoscaled areas are more intense in the unfiltered than in the 20-nm-filtered samples. The difference between 20-nm-filtered and unfiltered samples is greater for the oligomer pool compared with the dimeric species. Because of the lack of an internal reference species with time-independent area, the raw area data corresponding to oligomers were normalized in each spectrum using the overall β2m peak area sum. This normalization procedure can be considered an internal scaling of the experimental data sets, and thus the intensity values obtained thereof will be referred to as autoscaled intensities. It should be mentioned that, despite the mass conservation, comparisons among autoscaled intensities may be affected by systematic errors due to failure to observe in the mass spectrum large oligomeric species, especially for long aged samples.

compared with the corresponding control spectrum of β2m after 20 days in the absence of αB-crystallin (*F*). As is readily evident from inspection of Fig. 7, the presence of αB-crystallin potently inhibits the development of oligomeric β2m species. After 1 day (Fig. 7*B*), the mass spectrum of the mixture was essentially dominated by peaks from the monomer and dimer species and was highly comparable with the corresponding "time 0" spectrum of β2m on its own. In the absence of αB-crystallin, the corresponding spectrum of a β2m solution contained peaks arising from oligomeric species up to hexamers (data not shown). Furthermore, contrary to the spectrum of a 20-day-old solution of β2m, the spectrum of a 20-day-old mixture of β2m

and αB-crystallin did not exhibit any indication of conversion to large oligomeric β2m species.

Similar results were obtained using β2m/αB-crystallin molar subunit ratios of 30:1 and 90:1, with either unfiltered and filtered solutions. At a 90:1 β2m/αB-crystallin ratio, the sHsp was similarly effective at inhibiting the formation of β2m oligomers. Thus, MS demonstrates the impressive capacity of αB-crystallin, even at very low stoichiometric ratios, to completely inhibit the aggregation of wild-type β2m.

Fig. 8, *A* and *B*, shows the mass spectra of an aged (20-day-old) β2m solution at 1 and 20 days, respectively, after addition of αB-crystallin (at a 60:1 β2m/αB-crystallin ratio). The peaks corresponding to the oligomeric species that occur in aged β2m samples in the absence of αB-crystallin (Fig. 8*C*) are significantly decreased in its presence so that the mass spectrum of the aged β2m solution after 20 days of equilibration with αB-crystallin displays no oligomeric species and even a net decrease of the residual dimer peaks that were detected after a single day of equilibration with αB-crystallin. Importantly, the data in Fig. 8 provide compelling evidence for the capability of αB-crystallin to break down β2m oligomers in solution. In doing so, αB-crystallin converts β2m oligomers to monomers.

Similar MS experiments were conducted with two unrelated control proteins, GroEL, the well characterized molecular chaperone involved intimately with the folding of target proteins (for MS see ref. 63), and lysozyme, as representative of a typical medium-sized protein that has no chaperone ability. Independently of the molar subunit ratio (90 or 60 or 30:1 β2m/control) and preliminary solution filtering, none of the effects observed for αB-crystallin, *i.e.* prevention of β2m oligomerization and dissociation of β2m oligomers, was observed with GroEL (Fig. 9) or lysozyme (data not shown).

DISCUSSION

In this study, we have performed complementary NMR and MS experiments, addressing the very first stages of the β2m aggregation pathway and its inhibition due to interaction with the molecular chaperone αB-crystallin. We have previously shown that R3Aβ2m accumulates into fibrillar deposits in dialysis-related amyloidosis and exhibits a convenient aggregation time scale, while preserving all the features of the parent protein (19). Here, we have shown that R3Aβ2m forms fibrils at neutral pH upon agitation, a process that is inhibited by substoichiometric amounts of αB-crystallin.

We monitored the effect of αB-crystallin on R3Aβ2m in detail by NMR spectroscopy. First, we used ordinary solutions prepared from lyophilized R3Aβ2m, either unfiltered, centrifuged, or filtered through 0.22-μm filters. In the absence of α-crystallin, these samples exhibited a wide range of R3Aβ2m aggregation, precipitation, and unfolding behavior. Second, we used nonordinary R3Aβ2m solutions, *i.e.* solutions that were prepared under carefully controlled conditions, with un-lyophilized protein and filtered through 0.02-μm filters.

In ordinary samples of R3Aβ2m, aggregation was preceded by a lag phase that is consistent with the initial steps of the nucleated conformational conversion mechanism that R3Aβ2m undergoes during its aggregation (19). In the presence of αB-crystallin, the unfolding and aggregation of R3Aβ2m

M: monomer
D: dimer
T: trimer
Tt: tetramer
P: pentamer
Hex: hexamer
Hep: heptamer
Oct: octamer

F) β2m after 20 days

E) β2m and αB-Crystallin after 20 days

D) β2m and αB-Crystallin after 7 days

C) β2m and αB-Crystallin after 3 days

B) β2m and αB-Crystallin after 1 day
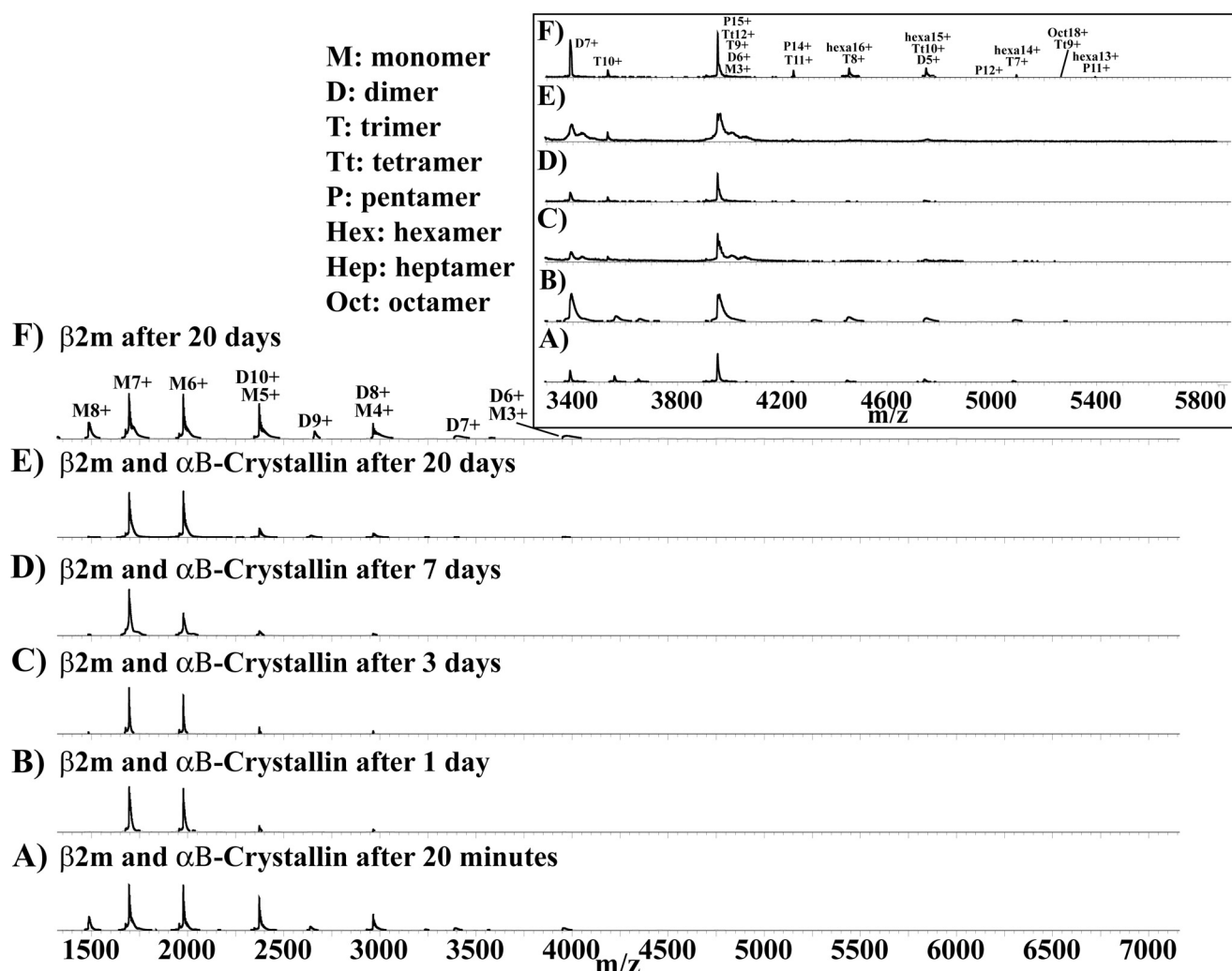
A) β2m and αB-Crystallin after 20 minutes

FIGURE 7. **Mass spectral monitoring of a solution containing simultaneously dissolved β2m and αB-crystallin (at a subunit molar ratio of 60:1) over 20 days (*A–E*) compared with the corresponding control spectrum of β2m after 20 days in the absence of αB-crystallin (*F*).**

were always substantially reduced implying that αB-crystallin interacts with R3Aβ2m at the earliest stages of its aggregation pathway, as we have observed for the interaction of αB-crystallin with other fibril-forming proteins, *e.g.* apolipoprotein C-II (42), α-synuclein (43, 50), and ataxin-3 (47).

In ordinary samples of R3Aβ2m, the lag phase prior to precipitation was 1 to several days, depending on the sample's concentration and previous history. Removing solute heterogeneity required filtered, un-lyophilized samples. These nonordinary samples enabled reproducible data to be obtained on the very early stages of aggregation.

NMR studies did not detect any protein aggregation or unfolding in the nonordinary samples of R3Aβ2m, even over extended time intervals. There was no specific interaction site of R3Aβ2m with αB-crystallin because a general dipolar broadening, associated with dipole-dipole interactions between closely spaced ^{1}H nuclei, was observed that affected the relaxation and increased the linewidths of R3Aβ2m resonances. It is therefore concluded that a large region of R3Aβ2m interacts with αB-crystallin. By evaluation of the backbone R3Aβ2m resonance attenuations, broadening was quantified, and the contacts between the two proteins were mapped (Fig. 3). β2m is a

protein that *in vivo*, apart from the fibrillar deposits in pathological conditions, normally occurs in complex with the polymorphic moiety of MHC-I. The finding that αB-crystallin is in contact with the regions that are involved in MHC-I assembly suggests the involvement of hydrophobic interactions in driving the association between R3Aβ2m and αB-crystallin. In our NMR examination of the interaction between α-synuclein and αB-crystallin, κ-casein and α-crystallin, and ataxin-3 and αB-crystallin, we also observed nonspecific association between the two proteins and a large region of interaction on the target protein (43, 47, 50). Thus, it would seem that αB-crystallin has a general, essentially entropy-driven mechanism of interaction with fibril-forming target proteins that involves transient, low affinity interactions with a large solvent-exposed region of the latter proteins. Another important feature of this interaction is that as a consequence of the weak transient contacts, the turnover efficiency leads to an extensive sampling of the target protein surface by the sHsp. This prerogative of sHsps is crucial for preventing the aggregation of the target proteins and appears to be a specific feature of sHsps when compared with the interaction of other molecular chaperones with target proteins. Thus, the failure of GroEL to prevent β2m oligomerization suggests
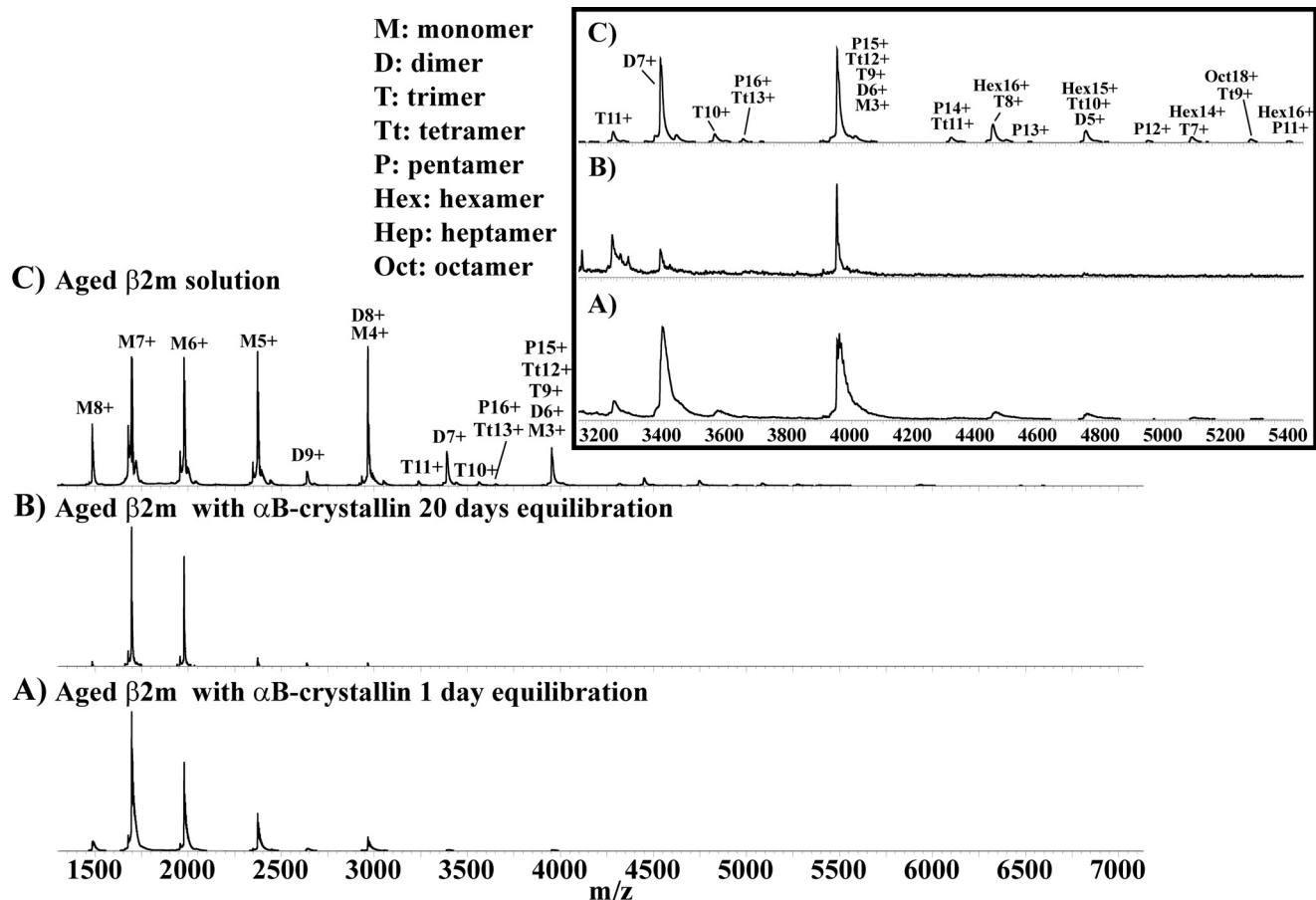
FIGURE 8. **ESI-MS of a 20-day-old wild-type β2m solution and αB-crystallin (60:1 β2m/αB-crystallin on a molar subunit basis) mixture, 1 day (*A*) and 20 days (*B*) after addition of αB-crystallin, in comparison with the control 20-day-old wild-type β2m solution (*C*).**

that it is not as versatile as sHsps in interacting with target proteins under stress conditions, *i.e.* it only interacts with target proteins along their folding pathway (9). The same inability of lysozyme ensures that the efficient, albeit nonspecific, chaperone action of sHsps cannot be attributed to a generic protein interaction.

The low affinity of αB-crystallin for β2m is an advantage in terms of preventing β2m aggregation. Most likely, the very potent chaperone ability of αB-crystallin, *i.e.* its ability to inhibit β2m aggregation at very low ratios of αB-crystallin to β2m, arises from the combination of the fast rate of transient binding and dissociation of αB-crystallin to β2m coupled with the slow process of unfolding of β2m toward an amyloidogenic conformation. Furthermore, at any one time, there are very few β2m molecules undergoing this unfolding process. As a result of these factors, a single αB-crystallin molecule can potentially contact multiple β2m molecules to stabilize the native β2m conformation. Contributing to αB-crystallin's high chaperone activity is its highly dynamic nature that arises from its inherent flexibility due to a large amount of structural disorder and its property of undergoing continuous subunit exchange. The ability of α-crystallin subunits to prevent amyloid fibril formation by wild-type β2m has been investigated at pH 2.5 under conditions in which β2m aggregates spontaneously (22). At this pH, α-crystallin subunits partially unfold and lose or have a significantly reduced oligomeric state (64, 65). No stable complex was

formed by either α-crystallin subunits with monomeric β2m (22), a conclusion in agreement with the results reported herein. Likewise, no complex is formed between α-crystallin and the fibril-forming protein, apolipoprotein C-II, although α-crystallin is a potent inhibitor of the latter's fibril formation (42). At acidic pH, the required concentration of chaperone for suppression of aggregation was nearly equal to that of β2m on a molar subunit basis (22). Under the conditions employed in this study (*i.e.* at neutral pH), the suppression of β2m fibril formation by αB-crystallin is much more efficient. The efficiency in our case can be explained in terms of the extremely low concentration of the dynamic β2m oligomers that are present at neutral pH, although the dissociation at acidic pH of the αB-crystallin oligomer and the concomitant unfolding of the monomer, which decrease the chaperone ability of αB-crystallin,[6] would have a significant effect on its ability to suppress β2m fibril formation.

An important observation from the MS studies presented herein is that αB-crystallin is capable of dissociating soluble wild-type β2m oligomers into monomers in aged β2m solutions incubated in the absence of αB-crystallin. Thus, αB-crystallin can dissociate soluble β2m oligomers into smaller species and thereby remove them from the fibril-forming, off-folding

---

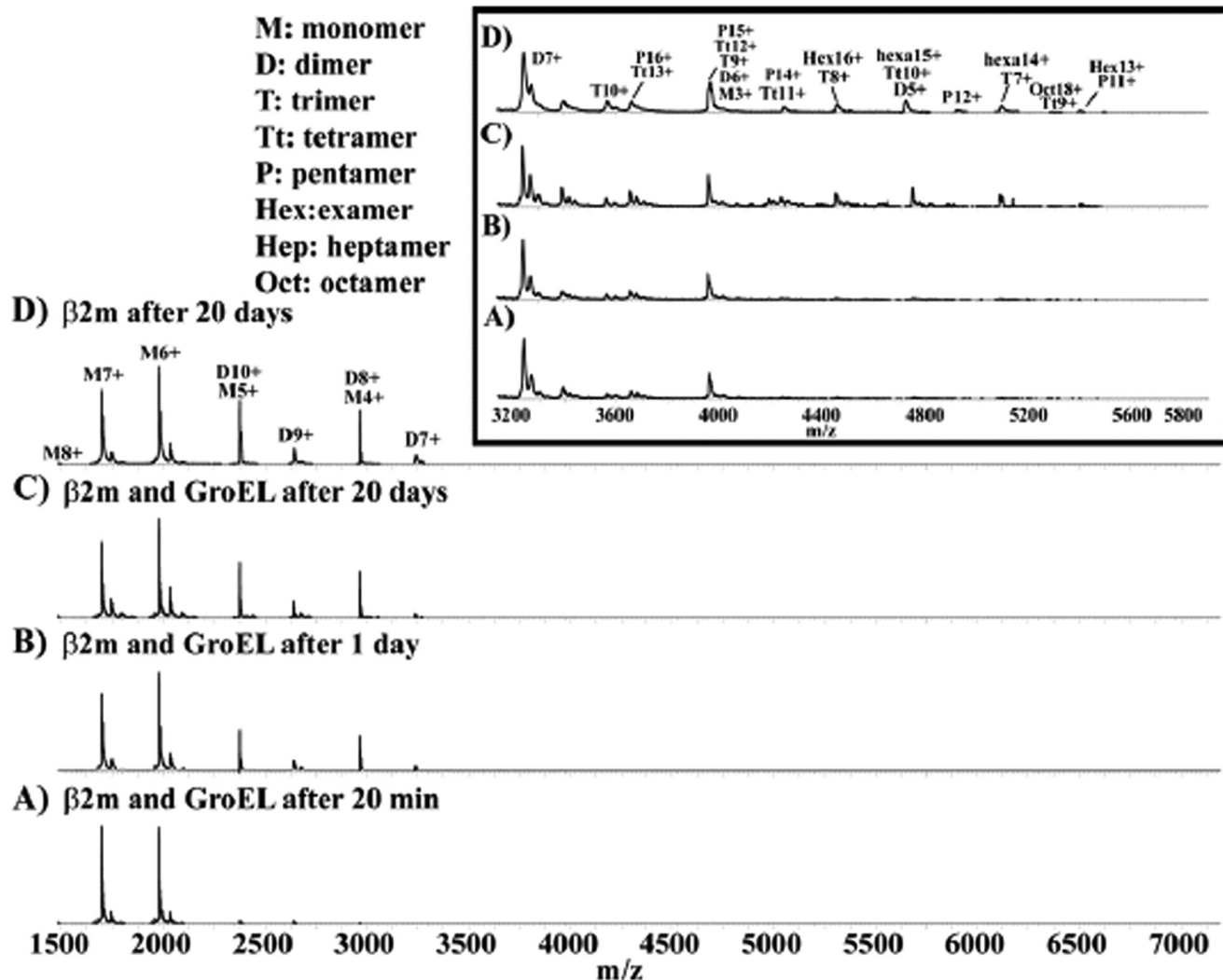[6] C. Brockwell, H. Ecroyd, and J. A. Carver, unpublished results.

M: monomer
D: dimer
T: trimer
Tt: tetramer
P: pentamer
Hex:examer
Hep: heptamer
Oct: octamer

FIGURE 9. Mass spectra of a β2m and GroEL mixture (molar ratio of 60:1 β2m/GroEL), 20 min (*A*), 1 day (*B*), and 20 days (*C*) after mixing the proteins together are shown. The mass spectrum of the 20-day-old β2m control solution is also reported (*D*). The data show clearly that GroEL has no effect on the β2m oligomerization process, *i.e.* the spectra at 20 days from solution preparation in the presence (*C*) and in the absence (*D*) of GroEL are highly comparable. Similar results were observed also at molar ratios 30:1 and 90:1 β2m/GroEL (data not shown).
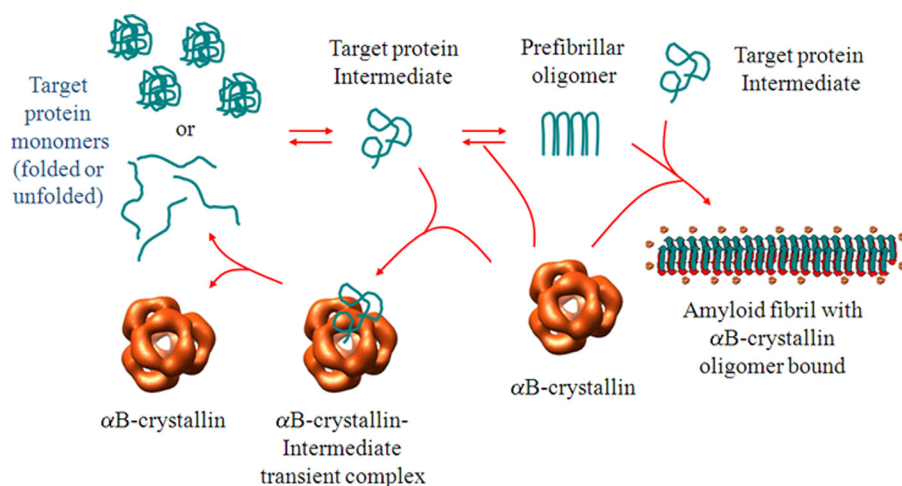

FIGURE 10. Schematic mechanism for the inhibition of amyloid fibril formation by αB-crystallin. During the formation of amyloid fibrils, target proteins (*e.g.* β2m), either folded or unfolded in their native state, can adopt a partially folded intermediate that is prone to aggregation to form prefibrillar oligomers. These can then sequester other intermediates to form the fibrillar species. αB-crystallin can interact with any of these species. Early along the aggregation pathway, *i.e.* at the intermediate or early oligomerization stage, αB-crystallin interacts transiently with the target protein and pushes it back into its monomeric, native conformation. It can also bind to the amyloid fibril to stabilize it and prevent its fragmentation and elongation.

pathway (9, 66, 67). As these oligomeric species are proposed to be cytotoxic, the ability of αB-crystallin to remove them is potentially of great importance in mitigating against their toxicity in diseases such as Alzheimer and Parkinson. Our results showing that αB-crystallin prevents the cellular toxicity of fibril-forming species, *e.g.* the Aβ peptide (41), is consistent with the ability of αB-crystallin to dissociate β2m oligomers.

Furthermore, our recent work has shown that αB-crystallin binds along the length and to the ends of fully formed amyloid fibrils of α-synuclein (50, 68), Aβ (69), and apolipoprotein C-II (70) to prevent fibril elongation and fragmentation. Fragmentation is recognized to be a major factor in fibril propagation due to it leading to secondary nucleation events and hence enhanced fibril formation (71).

The ability of αB-crystallin to interact with species at the various stages of the amyloid fibril-forming pathway is schematically represented in Fig. 10. The interaction at the early stages (with monomers and oligomers) is transient while binding of αB-crystallin to amyloid fibrils occurs (68–70). Thus, αB-crystallin is multifaceted in its ability to prevent fibril formation. Clearly, this multiplicity and plasticity in functionality provide αB-crystallin with enhanced capabilities *in vivo* in preventing the generation of toxic species arising from amyloid fibril formation and is consistent with the important role that αB-crystallin (and other sHsps) plays in minimizing protein aggregation.

REFERENCES

1. Chiti, F., and Dobson, C. M. (2006) Protein misfolding, functional amyloid, and human disease. *Annu. Rev. Biochem.* **75,** 333–366
2. Harper, J. D., Wong, S. S., Lieber, C. M., and Lansbury, P. T., Jr. (1997) Observation of metastable Aβ amyloid protofibrils by atomic force microscopy. *Chem. Biol.* **4,** 119–125
3. Lambert, M. P., Barlow, A. K., Chromy, B. A., Edwards, C., Freed, R., Liosatos, M., Morgan, T. E., Rozovsky, I., Trommer, B., Viola, K. L., Wals, P., Zhang, C., Finch, C. E., Krafft, G. A., and Klein, W. L. (1998) Diffusible, nonfibrillar ligands derived from Aβ1–42 are potent central nervous system neurotoxins. *Proc. Natl., Acad. Sci. U.S.A.* **95,** 6448–6453
4. Walsh, D. M., Klyubin, I., Fadeeva, J. V., Cullen, W. K., Anwyl, R., Wolfe, M. S., Rowan, M. J., and Selkoe, D. J. (2002) Naturally secreted oligomers of amyloid β protein potently inhibit hippocampal long-term potentiation *in vivo*. *Nature* **416,** 535–539
5. Hardy, J., and Selkoe, D. J. (2002) The amyloid hypothesis of Alzheimer's disease: progress and problems on the road to therapeutics. *Science* **297,** 353–356
6. Kayed, R., Head, E., Thompson, J. L., McIntire, T. M., Milton, S. C., Cotman, C. W., and Glabe, C. G. (2003) Common structure of soluble amyloid oligomers implies common mechanism of pathogenesis. *Science* **300,** 486–489
7. Yerbury, J. J., Kumita, J. R., Meehan, S., Dobson, C. M., and Wilson, M. R. (2009) α2-Macroglobulin and haptoglobin suppress amyloid formation by interacting with prefibrillar protein species. *J. Biol. Chem.* **284,** 4246–4254
8. Basha, E., O'Neill, H., and Vierling, E. (2012) Small heat shock proteins and α-crystallins: dynamic proteins with flexible functions. *Trends Biochem. Sci.* **37,** 106–117
9. Carver, J. A., Rekas, A., Thorn, D. C., and Wilson, M. R. (2003) Small heat-shock proteins and clusterin: intra- and extracellular molecular chaperones with a common mechanism of action and function? *IUBMB Life* **55,** 661–668
10. Saper, M. A., Bjorkman, P. J., and Wiley, D. C. (1991) Refined structure of the human histocompatibility antigen HLA-A2 at 2.6 Å resolution. *J. Mol. Biol.* **219,** 277–319
11. Gejyo, F., Yamada, T., Odani, S., Nakagawa, Y., Arakawa, M., Kunitomo, T., Kataoka, H., Suzuki, M., Hirasawa, Y., and Shirahama, T. (1985) A new form of amyloid protein associated with chronic hemodialysis was identified as β2-microglobulin. *Biochem. Biophys. Res. Commun.* **129,** 701–706
12. Verdone, G., Corazza, A., Viglino, P., Pettirossi, F., Giorgetti, S., Mangione, P., Andreola, A., Stoppini, M., Bellotti, V., and Esposito, G. (2002) The solution structure of human β2-microglobulin reveals the prodromes of its amyloid transition. *Protein Sci.* **11,** 487–499
13. Bellotti, V., Stoppini, M., Mangione, P., Sunde, M., Robinson, C., Asti, L., Brancaccio, D., and Ferri, G. (1998) β2-Microglobulin can be refolded into a native state from *ex vivo* amyloid fibrils. *Eur. J. Biochem.* **258,** 61–67
14. Esposito, G., Michelutti, R., Verdone, G., Viglino, P., Hernández, H., Robinson, C. V., Amoresano, A., Dal Piaz, F., Monti, M., Pucci, P., Mangione, P., Stoppini, M., Merlini, G., Ferri, G., and Bellotti, V. (2000) Removal of the N-terminal hexapeptide from human β2-microglobulin facilitates protein aggregation and fibril formation. *Protein Sci.* **9,** 831–845
15. Hoshino, M., Katou, H., Hagihara, Y., Hasegawa, K., Naiki, H., and Goto, Y. (2002) Mapping the core of the β2-microglobulin amyloid fibril by H/D exchange. *Nat. Struct. Biol.* **9,** 332–336
16. McParland, V. J., Kalverda, A. P., Homans, S. W., and Radford, S. E. (2002) Structural properties of an amyloid precursor of β2-microglobulin. *Nat. Struct. Biol.* **9,** 326–331
17. Eakin, C. M., Knight, J. D., Morgan, C. J., Gelfand, M. A., Miranker, A. D. (2002) Formation of a copper-specific binding site in non-native states of β2-microglobulin. *Biochemistry* **41,** 10646–10656
18. Villanueva, J., Hoshino, M., Katou, H., Kardos, J., Hasegawa, K., Naiki, H., and Goto, Y. (2004) Increase in the conformational flexibility of β2-microglobulin upon copper binding: a possible role for copper in dialysis-related amyloidosis. *Protein Sci.* **13,** 797–809
19. Corazza, A., Pettirossi, F., Viglino, P., Verdone, G., Garcia, J., Dumy, P., Giorgetti, S., Mangione, P., Raimondi, S., Stoppini, M., Bellotti, V., and Esposito, G. (2004) Properties of some variants of human β2-microglobulin and amyloidogenesis. *J. Biol. Chem.* **279,** 9176–9189
20. Naiki, H., Hashimoto, N., Suzuki, S., Kimura, H., Nakakuki, K., and Gejyo, F. (1997) Establishment of a kinetic model of dialysis-related amyloid fibril extension *in vitro*. *Amyloid Int. J. Exp. Clin. Invest.* **4,** 223–232
21. Kad, N. M., Myers, S. L., Smith, D. P., Smith, D. A., Radford, S. E., and Thomson, N. H. (2003) Hierarchical assembly of β2-microglobulin amyloid in vitro revealed by atomic force microscopy. *J. Mol. Biol.* **330,** 785–797
22. Raman, B., Ban, T., Sakai, M., Pasta, S. Y., Ramakrishna, T., Naiki, H., Goto, Y., and Rao, ChM. (2005) αB-crystallin, a small heat-shock protein, prevents the amyloid fibril growth of an amyloid β-peptide and β2-microglobulin. *Biochem. J.* **392,** 573–581
23. Yamamoto, S., Hasegawa, K., Yamaguchi, I., Tsutsumi, S., Kardos, J., Goto, Y., Gejyo, F., and Naiki, H. (2004) Low concentrations of sodium dodecyl sulfate induce the extension of β2-microglobulin-related amyloid fibrils at a neutral pH. *Biochemistry* **43,** 11075–11082
24. Yamamoto, S., Yamaguchi, I., Hasegawa, K., Tsutsumi, S., Goto, Y., Gejyo, F., and Naiki, H. (2004) Glycosaminoglycans enhance the trifluoroethanol-induced extension of β2-microglobulin-related amyloid fibrils at a neutral pH. *J. Am. Soc. Nephrol.* **15,** 126–133
25. Piazza, R., Pierno, M., Iacopini, S., Mangione P., Esposito, G., and Bellotti, V. (2006) Micro-heterogeneity and aggregation in β₂-microglobulin solutions: effects of temperature, pH, and conformational variant addition. *Eur. Biophys. J.* **35,** 439–445
26. Relini, A., Canale, C., De Stefano, S., Rolandi, R., Giorgetti, S., Stoppini, M., Rossi, A., Fogolari, F., Corazza, A., Esposito, G., Gliozzi, A., and Bellotti, V. (2006) Collagen plays an active role in the aggregation of β₂-microglobulin under physiopathological conditions of dialysis related amyloidosis. *J. Biol. Chem.* **281,** 16521–16529
27. Relini, A., De Stefano, S., Torrassa, S., Cavalleri, O., Rolandi, R., Gliozzi, A., Giorgetti, S., Raimondi, S., Marchese, L., Verga, L., Rossi, A., Stoppini, M., and Bellotti, V. (2008) Heparin strongly enhances the formation of β₂-

microglobulin amyloid fibrils in the presence of Type I collagen. *J. Biol. Chem.* **283,** 4912– 4920

28. Valleix, S., Gillmore, J. D., Bridoux, F., Mangione, P. P., Dogan, A., Nedelec, B., Boimard, M., Touchard, G., Goujon, J. M., Lacombe, C., Lozeron, P., Adams, D., Lacroix, C., Maisonobe, T., Planté-Bordeneuve, V., Vrana, J. A., Theis, J. D., Giorgetti, S., Porcari, R., Ricagno, S., Bolognesi, M., Stoppini, M., Delpech, M., Pepys, M. B., Hawkins, P. N., and Bellotti, V. (2012) Hereditary systemic amyloidosis due to Asp76Asn variant β2-microglobulin. *N. Engl. J. Med.* **366,** 2276 –2283

29. Bova, M. P., Ding, L. L., Horwitz, J., and Fung, B. K. (1997) Subunit exchange of αA-crystallin. *J. Biol. Chem.* **272,** 29511–29517

30. Sun, T. X., and Liang, J. J. (1998) Intermolecular exchange and stabilization of recombinant human αA- and αB-crystallin. *J. Biol. Chem.* **273,** 286 –290

31. Horwitz, J. (1992) α-Crystallin can function as a molecular chaperone. *Proc. Natl. Acad. Sci. U.S.A.* **89,** 10449 –10453

32. Bhat, S. P., and Nagineni, C. N. (1989) αB subunit of lens-specific protein α-crystallin is present in other ocular and non-ocular tissues. *Biochem. Biophys. Res. Commun.* **158,** 319 –325

33. Horwitz, J. (2000) The function of α-crystallin in vision. *Semin. Cell Dev. Biol.* **11,** 53– 60

34. Carver, J. A., Aquilina, J. A., Truscott, R. J., and Ralston, G. B. (1992) Identification by ¹H NMR spectroscopy of flexible C-terminal extensions in bovine lens α-crystallin. *FEBS Lett.* **311,** 143–149

35. Carver, J. A. (1999) Probing the structure and interactions of crystallin proteins by NMR spectroscopy. *Prog. Retin. Eye Res.* **18,** 431– 462

36. Carver, J. A., and Lindner, R. A. (1998) NMR spectroscopy of α-crystallin. Insights into the structure, interactions, and chaperone action of small heat-shock proteins. *Int. J. Biol. Macromol.* **22,** 197–209

37. Bagnéris, C., Bateman, O. A., Naylor, C. E., Cronin, N., Boelens, W. C., Keep, N. H., and Slingsby, C. (2009) Crystal structures of α-crystallin domain dimers of αB-crystallin and Hsp20. *J. Mol. Biol.* **392,** 1242–1252

38. Jehle, S., van Rossum, B., Stout, J. R., Noguchi, S. M., Falber, K., Rehbein, K., Oschkinat, H., Klevit, R. E., and Rajagopal, P. (2009) αB-crystallin: a hybrid solid-state/solution-state NMR investigation reveals structural aspects of the heterogeneous oligomer. *J. Mol. Biol.* **385,** 1481–1497

39. Laganowsky, A., Benesch, J. L., Landau, M., Ding, L., Sawaya, M. R., Cascio, D., Huang, Q., Robinson, C. V., Horwitz, J., Eisenberg, D. (2010) Crystal structures of truncated αA and αB crystallins reveal structural mechanisms of polydispersity important for eye lens function. *Protein Sci.* **19,** 1031–1043

40. Kudva, Y. C., Hiddinga H. J., Butler, P. C., Mueske, C. S., and Eberhardt, N. L. (1997) Small heat shock proteins inhibit *in vitro* Aβ(1– 42) amyloidogenesis. *FEBS Lett.* **416,** 117–121

41. Dehle, F. C., Ecroyd, H., Musgrave, I. F., and Carver, J. A. (2010) αB-crystallin inhibits the cell toxicity associated with amyloid fibril formation by κ-casein and the amyloid-β peptide. *Cell Stress Chaperones* **15,** 1013–1026

42. Hatters, D. M., Lindner, R. A., Carver, J. A., and Howlett, G. J. (2001) The molecular chaperone, α-crystallin, inhibits amyloid formation by apolipoprotein C-II. *J. Biol. Chem.* **276,** 33755–33761

43. Rekas, A., Adda, C. G., Andrew Aquilina, J., Barnham, K. J., Sunde, M., Galatis, D., Williamson, N. A., Masters, C. L., Anders, R. F., Robinson, C. V., Cappai, R., and Carver, J. A. (2004) Interaction of the molecular chaperone αB-crystallin with α-synuclein: effects on amyloid fibril formation and chaperone activity. *J. Mol. Biol.* **340,** 1167–1183

44. Ecroyd, H., Meehan, S., Horwitz, J., Aquilina, J. A., Benesch, J. L., Robinson, C. V., Macphee, C. E., and Carver, J. A. (2007) Mimicking phosphorylation of αB-crystallin affects its chaperone activity. *Biochem. J.* **401,** 129 –141

45. Treweek, T. M., Ecroyd, H., Williams, D. M., Meehan, S., Carver, J. A., and Walker, M. J. (2007) Site-directed mutations in the C-terminal extension of human αB-crystallin affect chaperone function and block amyloid fibril formation. *PLoS ONE* **2,** e1046

46. Ecroyd, H., and Carver, J. A. (2008) The effect of small molecules in modulating the chaperone activity of αB-crystallin against ordered and disordered protein aggregation. *FEBS J.* **275,** 935–947

47. Robertson, A. L., Headey, S. J., Saunders, H. M., Ecroyd, H., Scanlon, M. J.,

Carver, J. A., and Bottomley, S. P. (2010) Small heat-shock proteins inhibit polyglutamine aggregation by interactions with a flanking domain. *Proc. Natl. Acad. Sci. U.S.A.* **107,** 10424 –10429

48. Raman, B., Chatani, E., Kihara, M., Ban, T., Sakai, M., Hasegawa, K., Naiki, H., Rao, ChM., and Goto, Y. (2005) Critical balance of electrostatic and hydrophobic interactions is required for β2-microglobulin amyloid fibril growth and stability. *Biochemistry* **44,** 1288 –1299

49. Devlin, G. L., Carver, J. A., and Bottomley, S. P. (2003) The selective inhibition of serpin aggregation by the molecular chaperone, α-crystallin, indicates a nucleation-dependent specificity. *J. Biol. Chem.* **278,** 48644 – 48650

50. Rekas, A., Jankova, L., Thorn, D. C., Cappai, R., and Carver, J. A. (2007) Monitoring the prevention of amyloid fibril formation by α-crystallin: temperature dependence and nature of the aggregating species. *FEBS J.* **274,** 6290 – 6304

51. Garvey, M., Griesser, S. S., Griesser, H. J., Thierry, B., Nussio, M. R., Shapter, J. G., Ecroyd, H., Giorgetti, S., Bellotti, V., Gerrard, J. A., and Carver, J. A. (2011) Enhanced molecular chaperone activity of a small heat-shock protein following covalent immobilization onto a solid-phase support. *Biopolymers* **95,** 376 –389

52. Braunschweiler, L., and Ernst, R. R. (1983) Coherence transfer by isotropic mixing: application to proton correlation spectroscopy. *J. Magn. Reson.* **53,** 521–528

53. Molinari, H., Esposito, G., Ragona, L., Pegna, M., Niccolai, N., Brunne, R. M., Lesk, A. M., and Zetta, L. (1997) Probing protein structure by solvent perturbation of NMR spectra: the surface accessibility of BPTI. *Biophys. J.* **73,** 382–396

54. Koradi, R., Billeter, M., and Wüthrich, K. (1996) MOLMOL a program for display and analysis of macromolecular structure. *J. Mol. Graph.* **14,** 51–55

55. Jerschow, A, and Müller, N. (1998) Convection compensation in gradient enhanced nuclear magnetic resonance spectroscopy. *J. Magn. Reson.* **132,** 13–18

56. Piotto, M., Saudek, V., and Sklenár, V. (1992) Gradient-tailored excitation for single-quantum NMR spectroscopy of aqueous solutions. *J. Biomol. NMR* **2,** 661– 665

57. Hwang, T. L., and Shaka, A. J. (1995) Water suppression that works. Excitation sculpting using arbitrary waveforms and pulsed field gradients. *J. Magn. Reson.* **112,** 275–279

58. Floege, J., and Ketteler, M. (2001) β2-Microglobulin-derived amyloidosis: an update. *Kidney Int. Suppl.* **78,** S164 –S171

59. Yamamoto, S., and Gejyo, F. (2005) Historical background and clinical treatment of dialysis-related amyloidosis. *Biochim. Biophys. Acta* **1753,** 4 –10

60. Garvey, M., and Morgado, I. (2013) Peptide concentration alters intermediate species in amyloid β fibrillation kinetics. *Biochim. Biophys. Res. Commun.* **433,** 276 –280

61. Esposito, G., Lesk, A. M., Molinari, H., Motta, A., Niccolai, N., and Pastore, A. (1992) Probing protein structure by solvent perturbation of NMR spectra. II. Determination of surface and buried residues in homologous proteins. *J. Mol. Biol.* **224,** 659 – 670

62. Fischer, H., Polikarpov, I., and Craievich, A. F. (2004) Average protein density is a molecular-weight-dependent function. *Protein Sci.* **13,** 2825–2828

63. van Duijn, E., Bakkes, P. J., Heeren, R. M., van den Heuvel, R. H., van Heerikhuizen, H., van der Vies, S. M., and Heck, A. J. (2005) Monitoring macromolecular complexes involved in the chaperonin-assisted folding cycle by mass spectrometry. *Nat. Methods* **2,** 371–376

64. Meehan, S., Knowles, T. P., Baldwin, A. J., Smith, J. F., Squires, A. M., Clements, P., Treweek, T. M., Ecroyd, H., Tartaglia, G. G., Vendruscolo, M., Macphee, C. E., Dobson, C. M., and Carver, J. A. (2007) Characterisation of amyloid fibril formation by small heat-shock chaperone proteins, human αA-, αB-, and R120G αB-crystallins. *J. Mol. Biol.* **372,** 470 – 484

65. Horwitz, J. (2003) α-Crystallin. *Exp. Eye Res.* **76,** 145 –153

66. Treweek, T. M., Morris, A. M., and Carver, J. A. (2003) Intracellular protein unfolding and aggregation: the role of small heat-shock chaperone proteins. *Aust. J. Chem.* **56,** 357–367

67. Ecroyd, H., and Carver, J. A. (2009) Crystallin proteins and amyloid fibrils.

ASBMB

Cell. Mol. Life Sci. **66,** 62– 81

68. Waudby, C. A., Knowles, T. P., Devlin, G. L., Skepper, J. N., Ecroyd, H., Carver, J. A., Welland, M. E., Christodoulou, J., Dobson, C. M., and Meehan, S. (2010) The interaction of αB-crystallin with mature α-synuclein amyloid fibrils inhibits their elongation. *Biophys. J.* **98,** 843– 851

69. Shammas, S. L., Waudby, C. A., Wang, S., Buell, A. K., Knowles, T. P., Ecroyd, H., Welland, M. E., Carver, J. A., Dobson, C. M., and Meehan, S. (2011) Binding of the molecular chaperone αB-crystallin to Aβ amyloid fibrils inhibits elongation. *Biophys. J.* **101,** 1681–1689

70. Binger, K. J., Ecroyd, H., Yang, S., Carver, J. A., Howlett, G. J., and Griffin, M. D. (2013) Avoiding the oligomeric state: αB-crystallin inhibits fragmentation and induces dissociation of apolipoprotein C-II amyloid fibrils. *FASEB J.* **27,** 1214 –1222

71. Knowles, T. P., Waudby, C. A., Devlin, G. L., Cohen, S. I., Aguzzi, A., Vendruscolo, M., Terentjev, E. M., Welland, M. E., and Dobson, C. M. (2009) An analytical solution to the kinetics of breakable filament assembly. *Science* **326,** 1533–1537

Monitoring the Interaction between β₂-Microglobulin and the Molecular Chaperone αB-crystallin by NMR and Mass Spectrometry: αB-CRYSTALLIN DISSOCIATES β2-MICROGLOBULIN OLIGOMERS

Gennaro Esposito, Megan Garvey, Vera Alverdi, Fabio Pettirossi, Alessandra Corazza, Federico Fogolari, Maurizio Polano, P. Patrizia Mangione, Sofia Giorgetti, Monica Stoppini, Agata Rekas, Vittorio Bellotti, Albert J. R. Heck and John A. Carver

Access the most updated version of this article at doi: 10.1074/jbc.M112.448639

Alerts:
- When this article is cited
- When a correction for this article is posted

Click here to choose from all of JBC's e-mail alerts

This article cites 71 references, 16 of which can be accessed free at
http://www.jbc.org/content/288/24/17844.full.html#ref-list-1